Sorption and Transport of Inert Gases in PVF_2/PMMA Blends

J. S. CHIOU and D. R. PAUL, *Department of Chemical Engineering and Center for Polymer Research, University of Texas, Austin, Texas 78712*

Synopsis

Sorption and transport of several inert gases (He, Ar, N_2, and CH_4) in miscible blends of PMMA and PVF_2 are reported as a function of pressure at 35°C. For each gas, the permeabilities are independent of pressure for all blend compositions. Sorption isotherms are linear for rubbery compositions (PVF_2-rich) and nonlinear for glassy compositions (PMMA-rich) as expected. In contrast to CO_2, these gases do not plasticize any of these materials. The data are analyzed using appropriate models for sorption and transport, and the parameters are correlated in terms of blend composition and molecular characteristics of the gases. Effects of crystallinity are discussed. Sorption behavior is compared with poly(methyl acrylate) and poly(vinyl acetate).

INTRODUCTION

Sorption and transport of small molecules, like gases, in polymer blends has been the subject of numerous studies recently.[1-14] One can use the penetrant as a probe to investigate the phase structure of blends.[1-7] However, to employ this approach effectively, one must have some basis for understanding how sorption and transport in homogeneous mixtures relate to these characteristics for the individual components as recent work from our laboratory has attempted to establish experimentally[8,9,11-13] and theoretically.[14] Heterophase systems may be treated to a first approximation as composites[7] where the separate phases may stem from immiscibility or crystallinity.

Since sorption and transport responses differ depending on whether the polymer exists in the glassy or rubbery state,[15,16] one may expect more complicated analyses to be needed for miscible blends for which the T_g – composition relationship crosses the observation temperature as would be the case for the system poly(methyl methacrylate) (PMMA) and poly(vinylidene fluoride) (PVF_2) at 35°C. Furthermore, PMMA/PVF_2 blends may be completely amorphous for some compositions or have a varying fraction of crystallinity in other composition regions. We have completed a comprehensive investigation of this complex system. Carbon dioxide gas was found to cause significant plasticization of these blends leading to depression of T_g,[17] alteration of crystallinity,[18] modification of sorption isotherms,[19] and permeabilities which increase with pressure.[19] Here, we report results on the sorption and transport in these blends of several gases, He, Ar, N_2, and CH_4, which have considerably lower solubilities than CO_2; hence, the complications mentioned above[17-19] do not arise. The permeabilities for these gases are found to be independent of pressure even when the polymer is in the glassy state.[20]

Journal of Applied Polymer Science, Vol. 32, 4793–4814 (1986)
 CCC 0021-8995/86/054793-22$04.00

EXPERIMENTAL

The PVF_2 and PMMA used were commercial products designated as Kynar 460N by Pennwalt and Plexiglas V(811) by Rohm and Haas, respectively. Films of these two polymers and their blends were prepared by extrusion as described elsewhere.[17] The apparatus and procedures for sorption and permeation measurements were the same as described previously[21,22] except that no gas conditioning of the polymer was employed. The conditioning procedure was adopted for CO_2 sorption and permeation experiments to get reproducible results for subsequent measurements after the first cycle of experiments[23]; however, this was not needed for the present study as shown later.

Glass transitions, melting points, and crystallinity were measured by a differential scanning calorimeter (DSC) at a heating rate of 20°C/min. The onset temperature was taken as the T_g, and the apex temperature of the melting peak was defined as T_m. For blends containing less than 40% by weight of PVF_2, densities were measured at 30°C using a density gradient column based on aqueous solutions of calcium nitrate. Densities of blends containing 50% PVF_2 or more were so high that the preparation of solutions for the density gradient column was difficult. Therefore, an analytical balance using *n*-heptane as the buoyant fluid was used for these measurements.

RESULTS AND DISCUSSION

Characterization of Extruded Films

The glass transitions and the melting points of the as-extruded blends are shown in Figure 1, where the dashed line denotes the experimental temperature, 35°C, for this study. PVF_2 and the 80% PVF_2 blend have T_g's lower than 35°C and therefore are rubbery. All other compositions are glassy. Blends containing more than 50% PVF_2 are semicrystalline as shown from their melting peaks in the DSC. The melting points in Figure 1 are somewhat lower than those published previously[24-27] because of differences in the grades of polymer used and measuring techniques. The observed heat of fusion, ΔH_m, and the weight fraction crystallinity, X_c for each semicrystalline blend are listed in Table I, where 22.3 cal/g was taken as the ΔH_m for 100% crystalline PVF_2.[28] The volume fraction of the amorphous phase, α, blend was calculated by

$$\alpha = 1 - \rho X_c / \rho_{1,c} \tag{1}$$

where ρ is the density of the blend and $\rho_{1,c}$ (1 denotes PVF_2) is the density of the 100% crystalline PVF_2 taken as 1.873 g/cm^3.[29] The volume fraction of PVF_2 in the amorphous phase, ϕ_1, was calculated assuming volume additivity in the mixed amorphous phase

$$\phi_1 = \frac{V_{1,a}}{V_{1,a} + V_2} \tag{2}$$

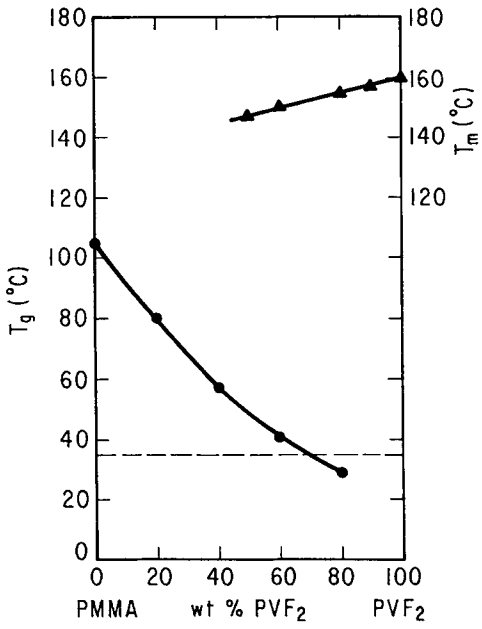

Fig. 1. Glass transition temperatures and melting points for extruded PVF_2/PMMA blends.

where $V_{1,a}$ is the volume of amorphous PVF_2 and V_2 is the volume of PMMA each expressed per unit mass of blend. The specific volumes of amorphous PVF_2[29] and of PMMA were taken as 0.5983 and 0.842 cm^3/g, respectively.

Sorption in PVF_2 and PMMA

Sorption isotherms for N_2, Ar, and CH_4 in PVF_2 and PMMA are shown in Figures 2 and 3, respectively. No results for He are given here because accurate measurements are difficult to obtain since the amount of sorption is so small. The sorption isotherms are reproducible over repeated cycles of measurement indicating no conditioning effect exists for these gas–polymer pairs. Henry's law is followed in Figure 2 since PVF_2 is rubbery at

TABLE I
Thermal and Volumetric Characteristics of as-extruded PVF_2/PMMA Blends

Wt % PVF_2	ΔH_m (cal/g)	X_c	ρ (g/cm^3)	α	ϕ_1
100	13.1	0.587	1.760	0.449	1.0
90	11.0	0.493	1.673	0.560	0.743
80	8.62	0.387	1.604	0.669	0.595
60	2.65	0.119	1.455	0.908	0.461
50	0.39	0.017	1.397	0.987	0.407
40	0	0	1.344	1.0	0.322
35	0	0	1.327	1.0	0.277
20	0	0	1.263	1.0	0.151
0	0	0	1.188	1.0	0

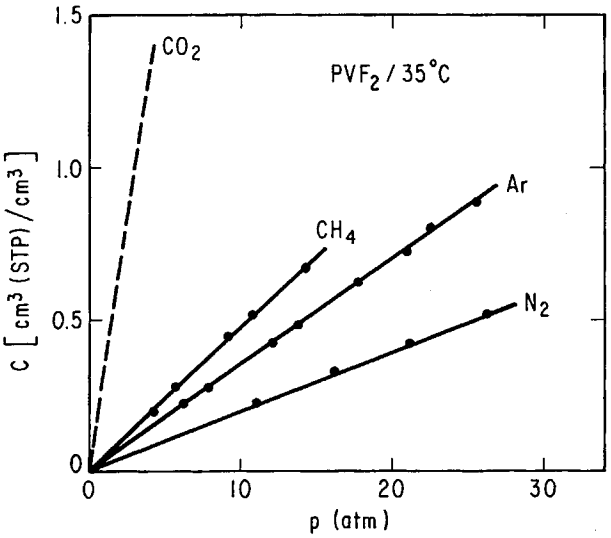

Fig. 2. Sorption isotherms for N_2, Ar, and CH_4 in PVF_2 at 35°C.

35°C, and the solubility coefficients, k_D taken from the slopes are listed in Table II. For PMMA, Figure 3 shows isotherms which are slightly concave to the pressure axis as expected for a glassy polymer. The isotherms follow the dual sorption equation

$$C = k_D p + \frac{C'_H bp}{1 + bp} \tag{3}$$

The solubility of these gases in PMMA is significantly lower than observed for higher T_g polymers like polycarbonate and polysulfone. For instance,

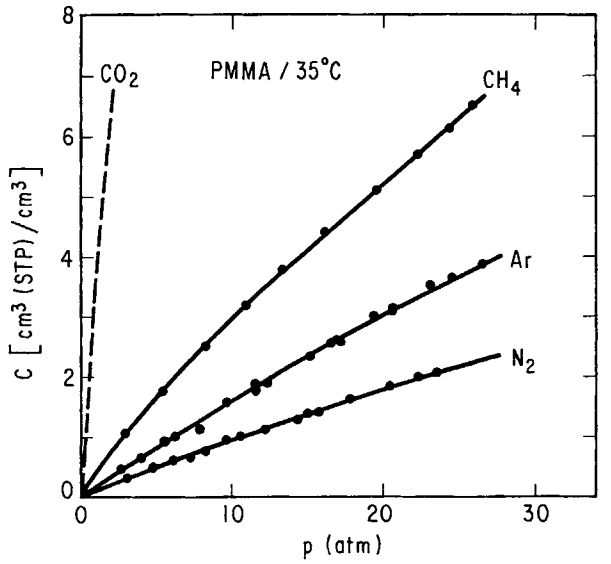

Fig. 3. Sorption isotherms for N_2, Ar, and CH_4 in PMMA at 35°C.

TABLE II
Henry's Law Coefficients for Gases in Extruded PVF_2 at 35°C

	k_D [cm³ (STP)/cm³ atm]				
	He	N_2	Ar	CH_4	CO_2
Sorption	—	0.0206	0.0350	0.0488	0.664[a]
Transport	0.0076[b]	0.0208	0.0392	0.0492	—

[a] Data from Ref. 19.
[b] Based on 7.0 mil film

the amount of sorption in PMMA at 20 atm is about two-thirds that in polycarbonate.[30] Furthermore, the isotherm curvature observed here is somewhat less, especially for Ar and N_2, indicating a smaller contribution from the second term in eq.(3). The sorption parameters k_D, C'_H, and b were obtained by fitting the data to eq. (3) by a computer regression program with the results shown in Table III. Sorption parameters for CO_2 obtained from other studies are also included in Tables II and III.

In an earlier paper, we reported that significant plasticization may occur when CO_2 is absorbed. For instance, the T_g of PMMA equilibrated at 35°C with CO_2 at 25 atm is reduced to 60°C from 105°C for the pure polymer.[17] The solubilities of He, Ar, N_2, and CH_4 are much lower than that of CO_2 as shown in Figures 2 and 3; therefore, their plasticizing effect is expected to be small. To confirm this, the T_g of PMMA which had been quenched from 170°C into ice water and then equilibrated at 35°C with 25 atm of Ar was measured by DSC. The experimental technique is described in the previous paper.[17] Comparison of the two thermograms in Figure 4 reveals that the T_g of PMMA was not depressed by the sorbed Ar to any significant extent. The hump at temperatures below T_g in scan A is due to sub-T_g annealing.[17] The fluctuations in scan A at temperatures higher than T_g are due to the desorption of Ar.

Sorption of Ar in Blends

Sorption isotherms for Ar in the various blends are shown in Figure 5. Straight lines are observed for the rubbery compositions while slightly concave curves are seen for the glassy ones. For the 60% PVF_2 blend, no curvature in the isotherm can be detected since its T_g is only slightly higher than the sorption temperature. The sorption parameters obtained from regression analysis are listed in Table IV. For the 40% PVF_2 blend,

TABLE III
Sorption Parameters for Various Gases in Extruded PMMA at 35°C

Gas	k_D [cm³ (STP/cm³ atm]	C'_H *[cm³ (STP)/cm³]*	b (atm^{-1})	$k_D + C'_H b$ [cm³ (STP)/cm³ atm]
N_2	0.0737	0.814	0.0301	0.0982
Ar	0.115	1.45	0.0480	0.185
CH_4	0.182	3.62	0.0560	0.385
CO_2[a]	1.41	25.6	0.0993	3.95

[a] From Ref. 19. Corrected for plasticization effects.

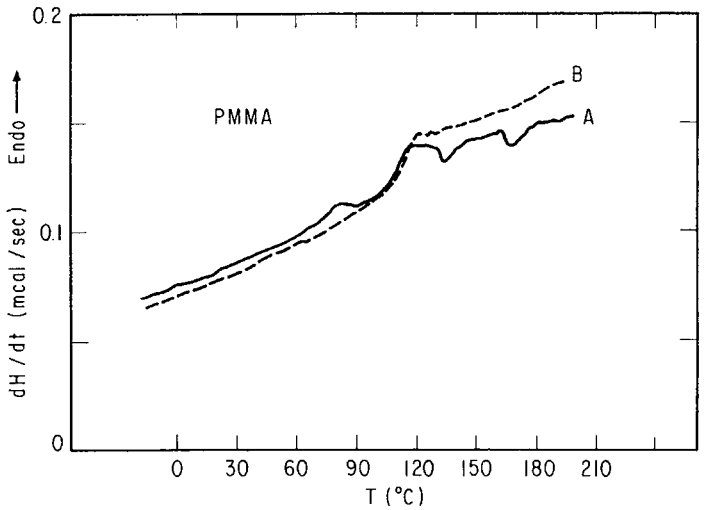

Fig. 4. DSC thermograms for PMMA: A was equilibrated with 25 atm of Ar prior to scan while B was not. Both show essentially the same T_g.

the curvature of the isotherm is very slight so that only the Henry's law coefficient calculated from the slope at high pressures is presented in Table IV.

The correlation between the Henry's law solubility coefficient and the blend composition is shown in Figure 6. For semicrystalline blends, the solubility coefficients have been divided by the factor α since sorption only occurs in the amorphous phase.[31,32] Earlier studies have suggested that the solubility coefficients for blends can be related to those of the component polymers by

$$\ln k_D = \phi_1 \ln k_{D,1} + \phi_2 \ln k_{D,2} + (BV_3/RT)\phi_1\phi_2 \quad (4)$$

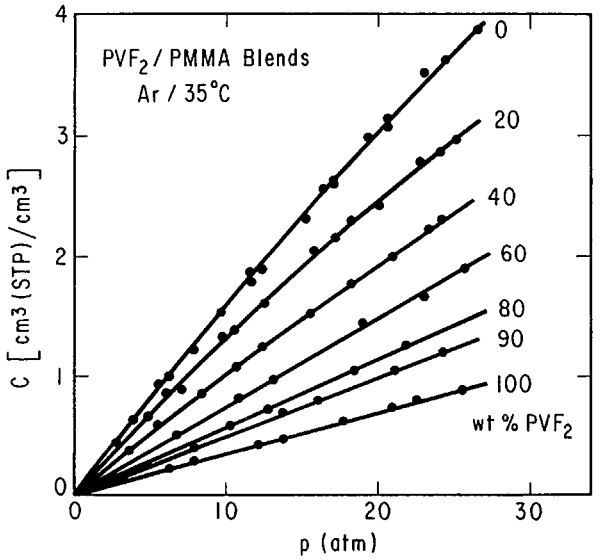

Fig. 5. Sorption isotherms for Ar in PVF_2/PMMA blends at 35°C.

TABLE IV
Sorption Parameters for Air in Extruded PVF_2/PMMA Blends at 35°C

Wt % PVF_2	k_D [cm^3 (STP)/ cm^3 atm]	C'_H [cm_3 (STP)/ cm^3]	b (atm^{-1})	k_D/α [cm^3 (STP)/ cm^3 atm]	k_D/α [10^{-3} cm^3 (STP)/ cm^3 cm Hg]
100	0.0350	—	—	0.0779	1.03
90	0.0480	—	—	0.0857	1.13
80	0.0568	—	—	0.0849	1.12
60	0.0742	—	—	0.0817	1.08
40	0.0893	—	—	0.0893	1.18
20	0.104	0.982	0.0345	0.104	1.37
0	0.115	1.45	0.0480	0.115	1.51

where B is the interaction energy density, V_3 is the molar volume of the gas, R is the gas constant, and subscripts 1 and 2 denote the two components. This equation has been successfully used to find the B value for miscible polymer blend systems.[8-12] A negative deviation from the tie line in Figure 6 is expected from eq. (4) since B is negative for a miscible blend. This is observed in Figure 6; however, there is significant scattering caused by experimental errors since the solubility levels are so low.[30] Solubility coefficients derived from permeation measurements are also shown in Figure 6 for comparison and similar scattering exists. A value for B of −3.85 cal/cm^3 obtained from melting point depression data[33] and V_3 = 57 cm^3/mol for Ar[34] were used to calculate the solid line in Figure 6. The measured and calculated results agree reasonably well.

Gas Transport in PVF_2 and PMMA

The diffusion coefficient D for a gas in a rubbery polymer can be determined from the diffusion time lag θ from a transient permeation experiment using

$$D = l^2/6\theta \tag{5}$$

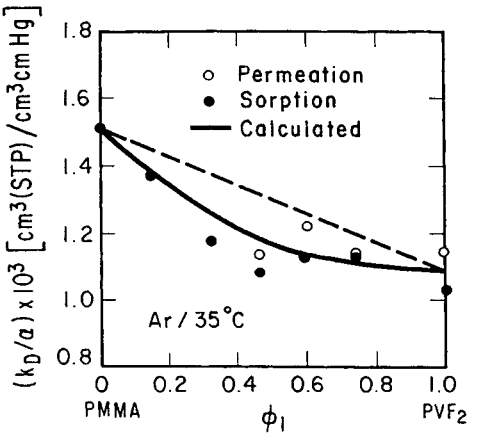

Fig. 6. Henry's law coefficient for Ar in blends at 35°C: calculated from eq. (4); (○) permeation; (●) sorption.

where l is the film thickness. The solubility coefficient k_D can be estimated from the ratio of the permeability coefficient P to D, i.e.,

$$k_D = P/D \tag{6}$$

Notice that these two equations are only valid when the diffusion coefficient is independent of concentration. This is the case here since the permeability coefficients for He, Ar, N_2, and CH_4 are independent of the upstream pressure, p_2, for all rubbery blends. Figure 7 shows an example for PVF_2. Similarly, the diffusion time lags for these gases in PVF_2 are also independent of p_2 as shown in Figure 8. The solubility coefficients determined from eq. (6) are listed in Table II to compare with the values measured directly from sorption experiments. The values from sorption and from permeation experiments agree within 10%.

The permeability coefficient for gases in glassy polymers may depend on pressure in a variety of ways. Most glassy polymers studied to date show permeability coefficients which decrease with pressure.[8,9,16,21,30,35-37] This response can be explained by a partial immobilization transport model,[38,39] in which the diffusion coefficient for the Henry's law mode is assumed constant and the mobility of the gas sorbed by Langmuir sites is a fraction of that dissolved in the polymer matrix. A few exceptional cases show permeability coefficients which increase with pressure.[19,40,41] In another paper,[19] we reported permeabilities for CO_2 in PVF_2–PMMA blends which increase with pressure owing to concentration dependent diffusion coefficients caused by CO_2 plasticization. Here, we note that the permeability coefficients for Ar, N_2, and CH_4 in PMMA-rich blends are independent of

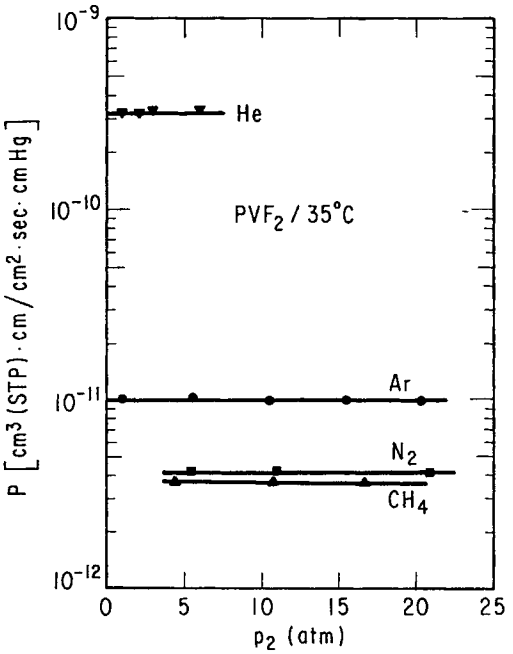

Fig. 7. Permeability coefficients for He, Ar, N_2, and CH_4 in PVF_2 at 35°C vs. pressure.

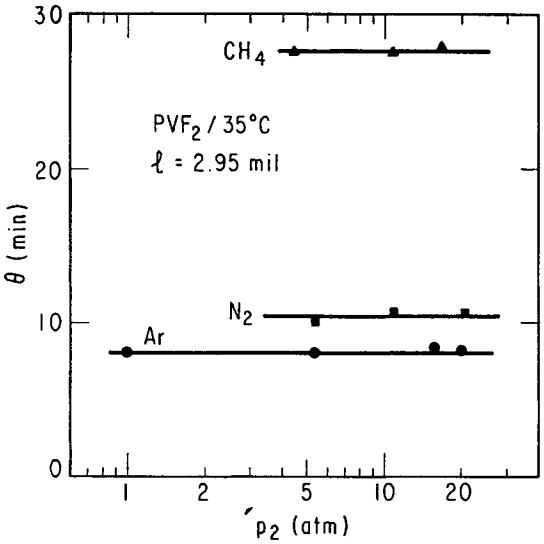

Fig. 8. Time lags for Ar, N_2, and CH_4 in PVF_2 at 35°C vs. pressure.

the pressure, as shown in Figure 9 for PMMA, within the range of experimental errors, 3%, from 1 to 20 atm.

Pressure independent permeability coefficients are expected when transport in a glass follows the *total* immobilization model[20]; however, such behavior has only been observed to date for model systems comprised of elastomers containing sorptive fillers.[42] While gas permeability coefficients in a glass can be pressure-independent like that in a rubber according to

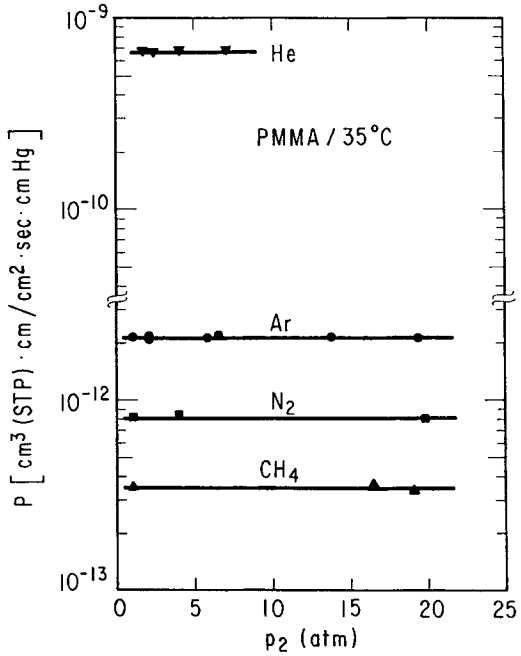

Fig. 9. Permeability coefficients for He, Ar, N_2, and CH_4 in PMMA at 35°C vs. pressure.

this model, an important means for distinguishing the former from the latter is that the time lag should decrease with pressure rather than be pressure independent. Figure 10 shows the measured time lags for Ar, N_2, and CH_4 in PMMA where a 20–40% decrease in θ is observed when the upstream pressure increases from 1 to 20 atm. According to the total immobilization transport model, the time lag can be calculated from the following:

$$\theta = \frac{l^2}{6D}[1 + Kf(bp_2)] \tag{7}$$

$$D = \frac{P}{k_D} \tag{8}$$

$$K = \frac{C'_H b}{k_D} \tag{9}$$

where $f(bp_2)$ is a function given previously.[20] The time lags calculated by this theory are also shown in Figure 10 for comparison.

Correlation of Blend Transport Behavior

Since the permeability coefficients for all blends studied here are independent of pressure, there is no need to choose a common pressure base to compare them with each other. The permeability coefficients for the four gases are plotted vs. overall blend composition in Figure 11. For Ar, N_2, and CH_4, the permeability coefficients increase with PVF_2 content up to 60% PVF_2 after which crystallinity begins to affect this relationship. The permeability to He is effectively independent of composition to this point but then decreases owing to increasing crystallinity. Apparent diffusion

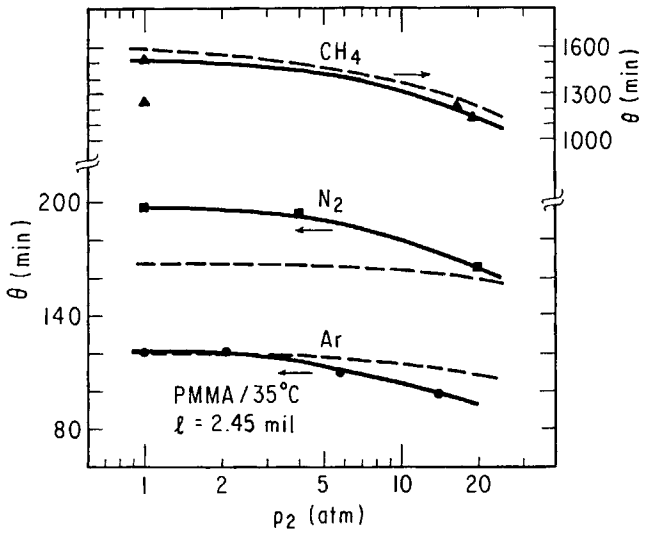

Fig. 10. Pressure dependence of diffusional time lags for Ar, N_2, and CH_4 in PMMA at 35°C: (- - -) calculated from eq. (7).

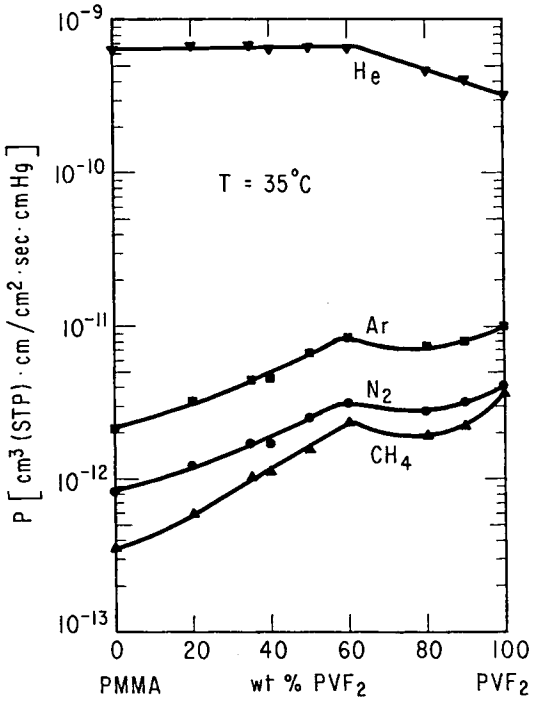

Fig. 11. Permeability coefficients for He, Ar, N_2, and CH_4 as a function of overall blend composition.

coefficients D_{app} computed from time lags using eq. (5) show responses rather similar to the permeability as seen in Figure 12. The value of D_{app} will depend on pressure (see Fig. 10), and those shown in Figure 12 are based on 20 atm. A "true" diffusion coefficient can be estimated from the total immobilization model [eqs. (7)–(9)] provided appropriate sorption information is known. Values estimated for Ar in this way are shown in Figure 12 for comparison, and on this scale the change in response seen is only slight. Similar information could not be computed for the other gases since their sorption isotherms were not measured.

For He, the diffusion time lags were too short (<4 s) in the standard films used for other gases to make reliable estimates of the diffusion coefficient. A few thicker films were prepared to obtain approximate He diffusion coefficients, and these are reported in Figure 12.

Blends containing 60% or more PVF_2 are significantly crystalline as shown in Table I, which tends to reduce both P and D relative to purely amorphous compositions. This effect is clearly seen in Figures 11 and 12. Since crystals act as barriers to gas transport, the effective diffusion coefficient computed by the methods used above is less than that in the amorphous phase by a factor κ.[31,43] Based on composite theory,[7] κ is a function of both the level of crystallinity and the crystalline morphology. In order to compare diffusion behavior of the crystalline blends with amorphous blends ($<50\%$ PVF_2), some means of adjusting the data for the κ factor is needed. It has been suggested that an upper bound on κ is obtained by equating it to the amorphous volume fraction, i.e.,

$$\kappa \simeq \alpha \tag{10}$$

We have done this in Figure 13 since no better alternative was available. Based on a simple rule of mixtures, one may expect the diffusion coefficients for blends to follow

$$\ln D = \phi_1 \ln D_1 + \phi_2 \ln D_2 \tag{11}$$

which using the coordinates in Figure 13 should result in a continuous straight line over the entire range of compositions. Instead, there is a break dividing the completely amorphous and glassy compositions from those which are semicrystalline and rubbery. We feel that a major reason for this is that κ is probably less than the estimate provided by eq. (10), which fails to raise the values of the diffusion coefficient in the semicrystalline region to become an extension of those from the fully amorphous region. In fact, based on a recent theory,[14] one might expect a relation which is concave upwards rather than linear as suggested by eq. (11). However, the situation for these blends is too complex to push the analysis further.

As a final point, we attempt to assess the influence of varying crystallinity on the relationship between permeability and blend composition. The solubility part of P should be proportional to α and again using eq. (10) for the mobility part suggests plotting P/α^2 vs. the composition of the amorphous phase as shown in Figure 14. Once more a break in the relation for

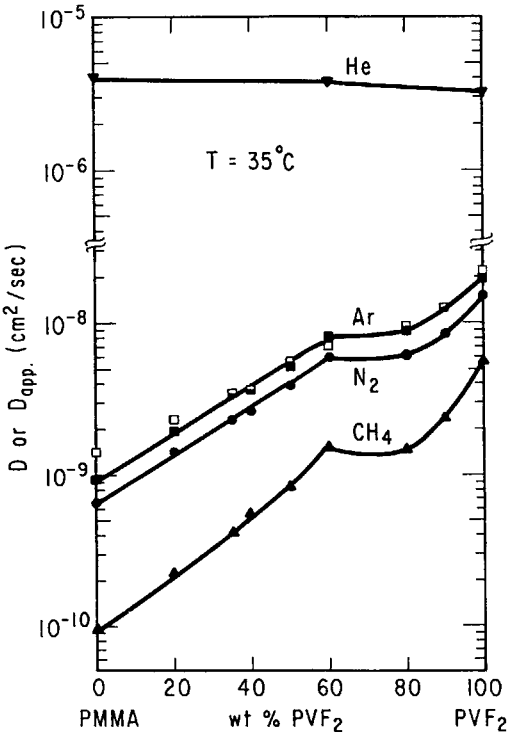

Fig. 12. Diffusion coefficients for He, Ar, N_2, and CH_4 as a function of overall blend composition. All data points except for the open squares were computed from $l^2/6\theta$: (□) for Ar, calculated from $D = P/k_D$.

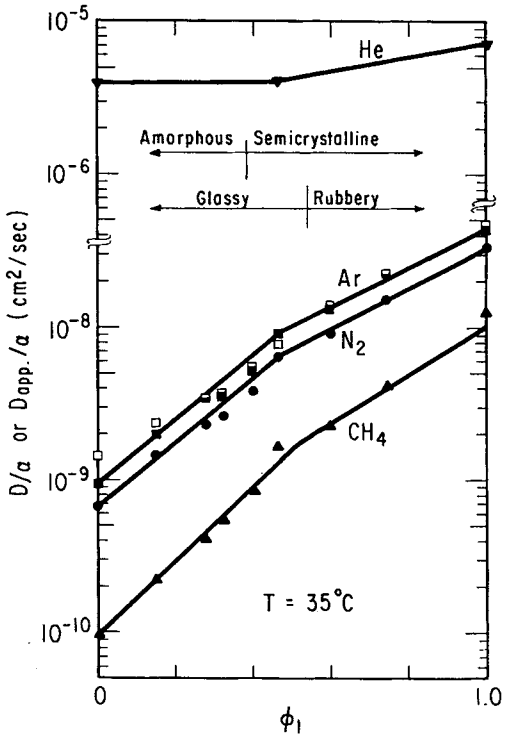

Fig. 13. Diffusion coefficients divided by the amorphous volume fraction as a function of PVF_2 volume fraction in amorphous phase. Symbols are the same as in Figure 12.

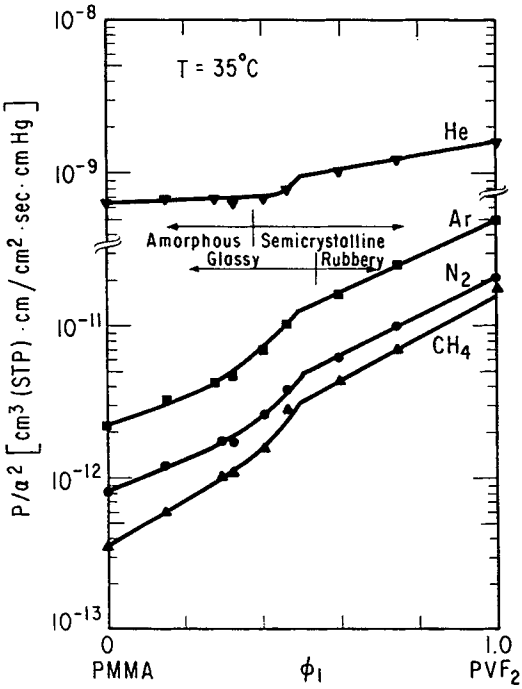

Fig. 14. Permeability coefficients divided by the square of amorphous phase volume fraction as a function of PVF_2 volume fraction in amorphous phase.

each gas appears in the region separating amorphous and glassy compositions from those which are semicrystalline and rubbery, which precludes comparisons with simple mixing rules.[14] The crude approximation eq. (10) provides is at least one reason for this.

Correlation of Sorption Parameters

Earlier studies have shown that all three sorption parameters in eq. (3) can be correlated to the Lennard–Jones potential well depth ϵ/κ by a semilogarithmic relationship.[8,30,37] Figures 15 and 16 show such plots for the Langmuir site capacity C'_H and the hole affinity constant b for pure PMMA. There is a good linear correlation in both cases. The Henry's law coefficients k_D for both PMMA and PVF_2 are plotted vs. ϵ/κ in Figures 17 and 18. For PVF_2, k_D values obtained from both sorption and permeation experiments were used. In the past[16,32,44] we have found a relation of the form

$$\log k_D = \log k_D^0 + m(\epsilon/\kappa) \tag{12}$$

to describe data for other polymers in either the rubbery or glassy states. The value of m is always close to 0.0095 K^{-1} while k_D^0 will vary considerably more depending on the polymer.[16,44] The dashed straight lines in Figures 17 and 18 have been drawn with a slope $m = 0.0095$ and a choice of k_D^0 to maximize the fit to the data. In every case, CO_2 falls above this line by a substantial amount as also reported recently for PVC.[45] For PMMA, data for all gases except CO_2 agree well with the line drawn giving $k_D^0 = 0.0093$ cm^3 (STP)/cm^3 atm, which is typical of many polymers.[44] For PVF_2, the He point lies above the line drawn, which may reflect errors in measuring its time lag as described earlier or a correlation line of lower slope. The value of k_D^0 obtained from the line drawn for PVF_2, 0.0026 cm^3 (STP)/cm^3

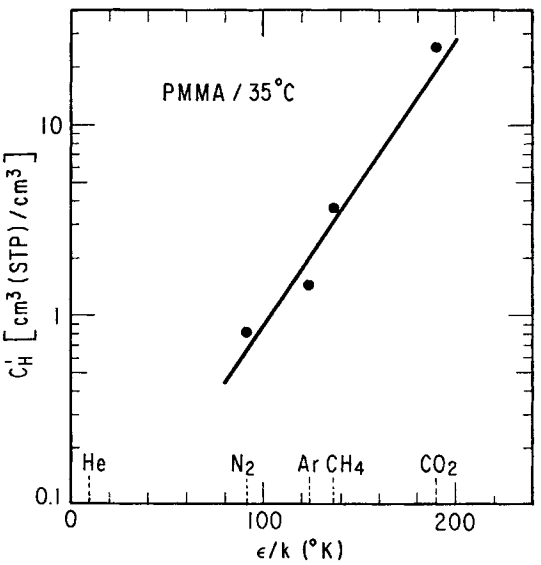

Fig. 15. Correlation of Langmuir capacity terms for PMMA with Lennard–Jones potential well depth of the gas.

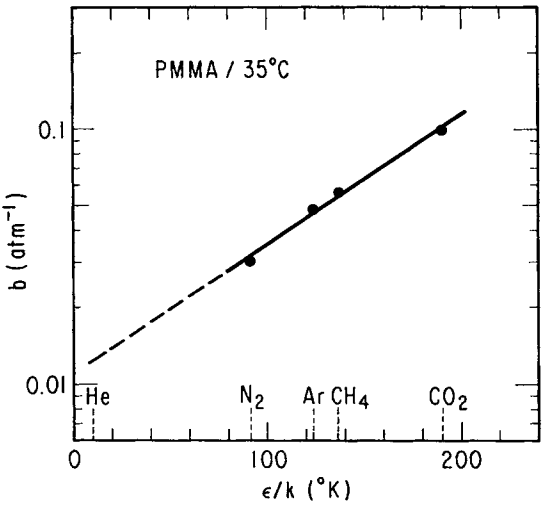

Fig. 16. Correlation of affinity constant for PMMA with Lennard–Jones potential well depth of the gas.

atm, is smaller than for most polymers but larger than a recently reported value of 0.002 cm^3 (STP)/cm^3 atm for PVC.[45]

To explore further the issues shown in Figures 17 and 18, we have examined the analogous behavior for poly(methyl acrylate) and poly(vinyl acetate) which are isomers and similar to PMMA by each having COO linkages in their pendant groups. Data from this work and four other sources[46–49] are plotted vs. ϵ/κ in Figure 19. The results for PMA and PVAc

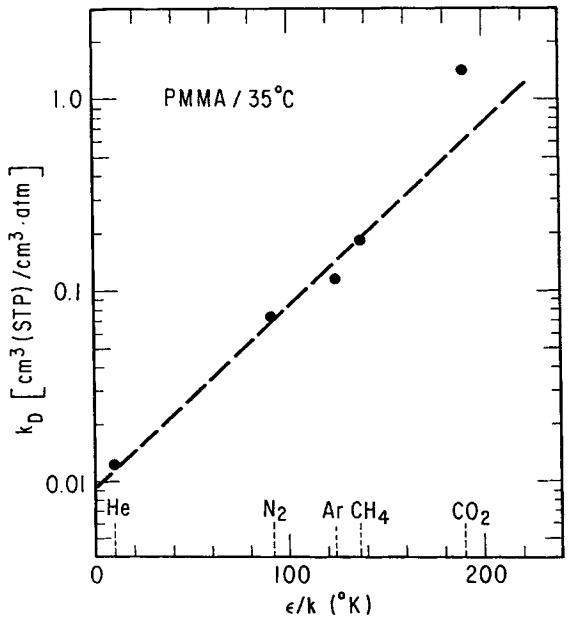

Fig. 17. Correlation of Henry's law constant k_D for PMMA with Lennard–Jones potential well depth of the gas. Data point for He from permeation measurements, the others from sorption measurements.

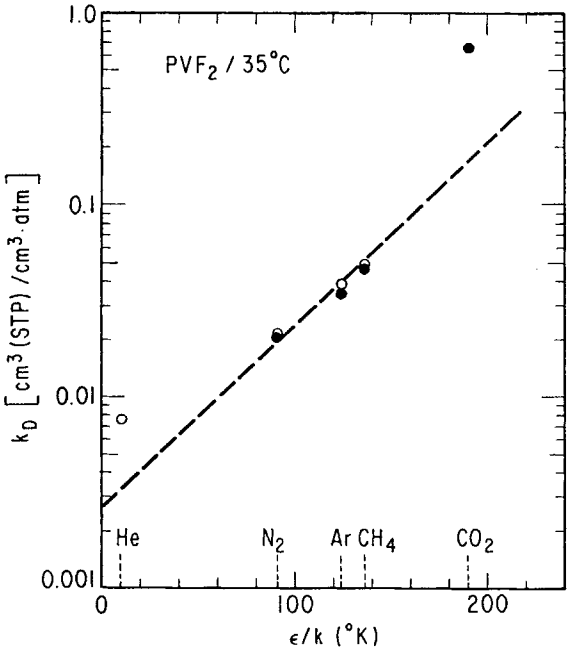

Fig. 18. Correlation of Henry's law constant k_D for PVF_2 with Lennard–Jones potential well depth of the gas: (○) from permeation measurements; (●) from sorption isotherms.

are essentially identical which is somewhat expected in view of their very similar structures. Again a straight line has been drawn with slope $m = 0.0095\ K^{-1}$ with k_D^0 adjusted to maximize the fit with the data. Some points for He and H_2 fall slightly above the line for reasons which are not clear to us. As seen for PMMA and PVC, CO_2 falls well above the line, which

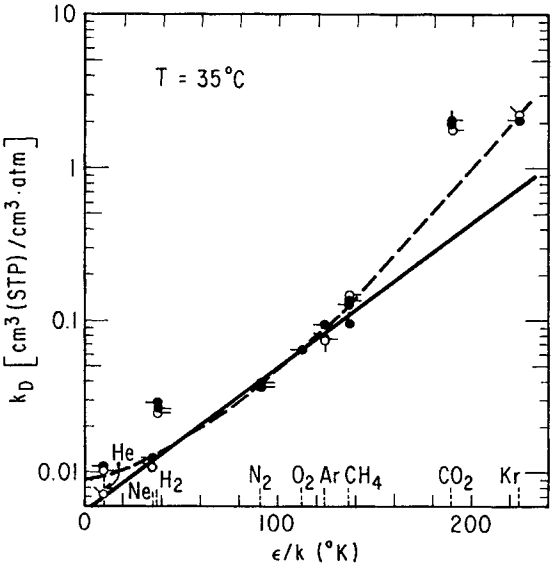

Fig. 19. Correlation of Henry's law constants k_D for poly(methyl acrylate) (○) and poly(vinyl acetate) (●) with Lennard–Jones potential well depth of the gas. The bars on data points denote the data source: (up) Ref. 49; (right) this work; (left) Ref. 46; (down) Ref. 48; (up-left) Ref. 47.

has been suggested to result from some specific interaction between CO_2 and the polymer. It is interesting to note that Kr also lies above the line in Figure 19 but not as far away as CO_2. The main point established here is that CO_2 seems to have an exceptionally large Henry's law solubility coefficient in some polymers, e.g., PVC, PMMA, PMA, and PVAc, compared to others.[16,30,32,44,45] The observation for Kr in Figure 19 may justify using a curve instead of a straight line in Figure 19; however, even then CO_2 would lie well above such a curve as suggested by the dashed line in Figure 19. This unusual solubility effect for CO_2 is being explored further. Enhanced CO_2 solubility has been reported for butadiene/acrylonitrile copolymers.[50] The higher H_2 solubility than expected remains a puzzle.

Correlation of Diffusion Coefficients

Gas diffusion coefficients in polymers may be correlated with the molecular size of the diffusing molecule, and the Lennard–Jones collision diameters[51] are often used for this purpose. Figure 20 shows a plot of the observed diffusion coefficients for PVF_2 vs. the Lennard–Jones collision diameter of the gas molecules. A smooth curve seems to describe the data for the three spherical gases, He, Ar, and CH_4; however, for N_2 and CO_2, which are more linear in molecular shape, their diffusion coefficients lie above this correlation line. In fact, a parallel study[52] using a commercial PVF_2 film has shown that H_2 and O_2 also behave like N_2 and CO_2 in this respect, and a very good correlation curve lying above that for spherical gases can be established for these linear gases. This indicates that rotational freedom may be somewhat restricted for these gases as they make diffusional jumps in the polymer.

For glassy polymers, previous studies using polycarbonate,[30] polysulfone,[37] and a copolyester[8] have shown that the diffusion coefficient for CO_2

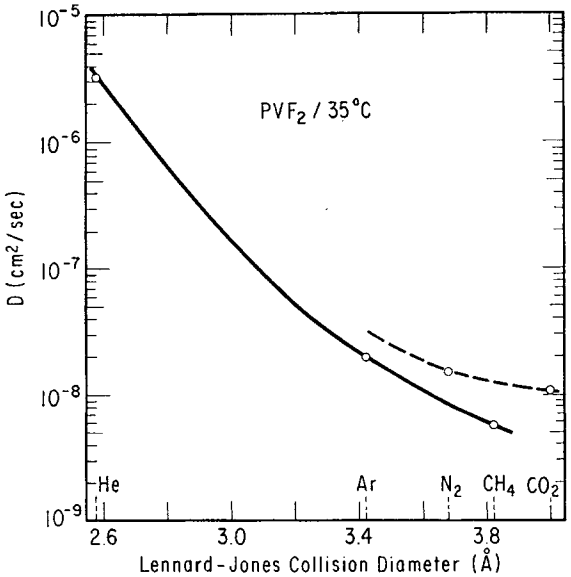

Fig. 20. Correlation of diffusion coefficients in PVF_2 with Lennard–Jones collision diameter of the gas.

lies well above the correlation curve if Lennard–Jones collision diameters are used. However, if kinetic diameters measured from zeolite sorption[53] are used, the correlation is quite satisfactory. Note that CO_2 has a kinetic diameter of 3.3 Å, which is much smaller than its collision diameter of 4.00 Å. For the other gases studied here, however, the kinetic and collision diameters are very close (see the abscissas of Figs. 20 and 21). Thus, it was suggested that diffusional jump of CO_2 in mobility restricted environments must occur without significant rotation of the CO_2 molecule.[30] This argument is examined in Figure 21 for PMMA, where the diffusion coefficients are plotted vs. the kinetic diameters. The diffusion coefficient for CO_2 is based on measurements for a film exposed to a CO_2 pressure of 1 atm and no higher.[19] The correlation curves for spherical and linear gases in Figure 21 are similar to those in Figure 20 except CO_2 falls below the correlation curve. A parallel study[52] for PMMA has shown that for CO_2 the data point can be better correlated if the collision diameter is used instead of the kinetic diameter. The different correlation behavior of CO_2 in PMMA from the three polymers studied before[8,30,37] might result from the different molecular structures of the polymers. While PMMA has a large pendent group, polycarbonate, polysulfone, and the polyester all have rigid backbones without pendent groups. Further studies of gas transport in other poly(alkyl methacrylate)s which are underway should give more conclusive results on this point.

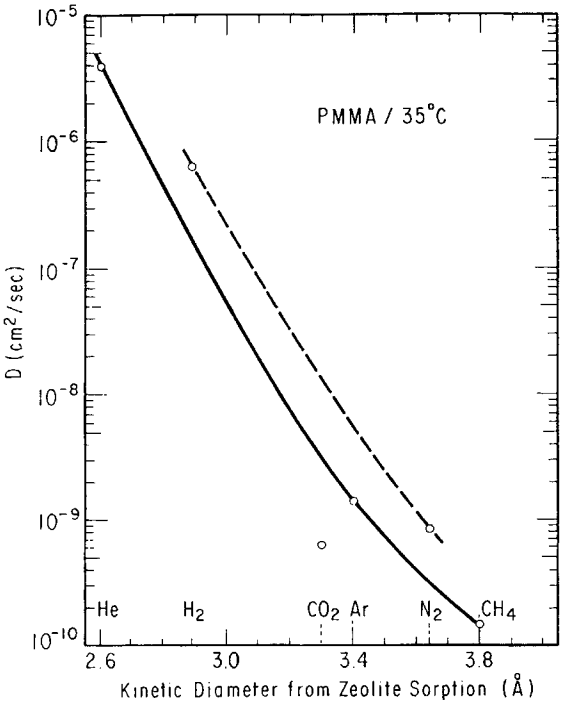

Fig. 21. Correlation of diffusion coefficients in PMMA with kinetic diameter of the gas. Apparent diffusion coefficients are given for He and H_2, and the ratio of permeability to solubility coefficient at 1 atm is used for CO_2.

Ideal Separation Factors

Owing to the interest in using polymer membranes for gas separations, we will examine the potential of these materials for separations. An ideal separation factor for gas A relative to gas B is given by the ratio of permeabilities to these gases, i.e.

$$\alpha_B^A = P_A/P_B \tag{13}$$

Use of pure gas permeabilities ignores any interactions between gases during transport of a mixture. We will examine the ideal separation factors for He/CH_4, CO_2/CH_4, and H_2/CH_4 owing to the practical significance of separating these pairs. Calculated ratios of permeabilities are shown in Figure 22. Only a single value for H_2/CH_4 is given since H_2 permeability was measured only for PMMA.

The ideal separation factors show a change in character at 60% PVF_2 where crystallinity becomes significant. Interestingly, these effects do not cancel from the permeability ratio which suggests that κ probably depends on gas type in addition to morphology and level of crystallinity. Composite theory would not predict this. Since CO_2 permeability depends on pressure, the value of $\alpha_{CH_4}^{CO_2}$ computed will vary according to the pressure selected — 20 atm is used here. Very likely, plasticization by CO_2 will alter the actual separation factor which can only be determined by mixed gas measurements which were not done. Ignoring this, extraordinarily high separation factors are seen for all gas pairs in PMMA rich blends. For PMMA, $\alpha_{CH_4}^{CO_2}$ is 230, which is in contrast to values in the range of 10–40 for many other polymers.[49] Likewise, $\alpha_{CH_4}^{He}$ is much higher for PMMA than most other polymers. This is because the He diffusion coefficient is about 3×10^4 larger than

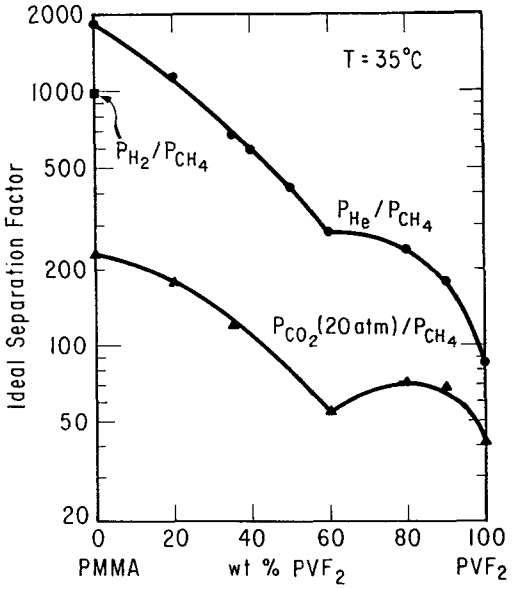

Fig. 22. Ideal separation factors for gas pairs vs. blend compositions.

that for CH_4; however, the He solubility coefficient is only about a factor of 15 less than that for CH_4. On the other hand, for CO_2/CH_4 in PMMA, the ratio of diffusion coefficients (~30) and solubilities (~8) both favor transport of CO_2 over CH_4.

The peculiar shape of the separation factors vs. blend composition seen in Figure 22 can be understood by comparing the different shapes of the plots for He and CH_4 permeability in Figure 11 and for CO_2 in Figure 23.[19]

SUMMARY

The miscible blend system PMMA/PVF_2 consists of totally amorphous, glassy materials on the PMMA side of the composition scale while semicrystalline, rubbery materials exist on the PVF_2 side. The change from glassy to rubbery materials as composition is varied is reflected in the shape of the sorption isotherms of gases and the effect pressure has on the diffusion time lags. The appearance and variation of crystallinity as the PVF_2 content increases affects both gas solubility and permeation in these blends. Because of these complexities, it is not possible to analyze the effect of blend composition on these characteristics using the simple relations which have been shown to apply to homogeneous miscible blends[14] which are always glassy[8,9,13] or always rubbery.[12]

Simple procedures to estimate gas solubility in the amorphous phase of semicrystalline mixtures seem to work well; however, similar estimates for diffusion coefficients or permeability coefficients in the amorphous phase are not as good. The variation of Ar solubility with blend composition corrected for crystallinity is entirely consistent with theoretical estimates.

The sorption and transport of He, Ar, N_2, and CH_4 in these blends is considerably less complicated than that described earlier for CO_2[19] since the latter plasticizes the polymers while the former do not.

PMMA exhibits some unique gas sorption and transport behavior com-

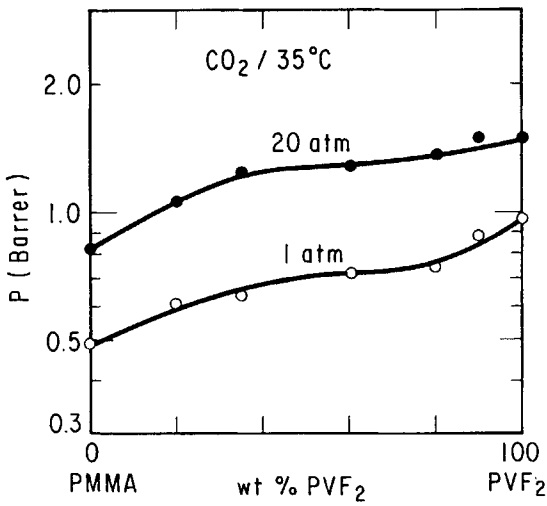

Fig. 23. Permeability coefficients for CO_2 plotted vs. blend composition. Data are from Ref. 19.

pared with other glassy polymers studied previously. For gases like He, Ar, N_2, and CH_4 the permeability is independent of pressure for PMMA whereas these permeabilities decrease with pressure to varying degrees in these other polymers. The permeability to CO_2 increases with pressure for PMMA while it decreases with pressure the same as other gases in many glassy polymers. PMMA shows what appears to be unusually selective gas permeation. Clearly, further studies on the effect of polymer structure on gas sorption and transport behavior are needed to fully understand these issues and are crucial to the development of advanced membrane materials for separations.

This research was supported by the U. S. Army Research Office.

References

1. B. G. Ranby, *J. Polym. Sci., Symp. Ed.*, **51**, 89 (1975).
2. Y. J. Shur and B. Ranby, *J. Appl. Polym. Sci.*, **19**, 1337 (1975).
3. Y. J. Shur and B. Ranby, *J. Appl. Polym. Sci.*, **19**, 2143 (1975).
4. Y. J. Shur and B. Ranby, *J. Appl. Polym. Sci.*, **20**, 3105 (1976).
5. Y. J. Shur and B. Ranby, *J. Appl. Polym. Sci.*, **20**, 3121 (1976).
6. Y. J. Shur and B. Ranby, *J. Macromal. Sci. Phys.*, **B14**, 565 (1977).
7. H. B. Hopfenberg and D. R. Paul in *Polymer Blends*, D. R. Paul and S. Newman, Eds., Academic, New York, 1978, Vol. I, Chap. 10.
8. P. Masi, D. R. Paul, and J. W. Barlow, *J. Polym. Sci., Polym. Phys. Ed.*, **20**, 15 (1982).
9. G. Morel and D. R. Paul, *J. Membr. Sci.*, **10**, 273 (1982).
10. H. G. Spencer and J. A. Yavorsky, *J. Appl. Polym. Sci.*, **28**, 2937 (1983).
11. J. E. Harris, D. R. Paul, and J. W. Barlow, *Polym. Eng. Sci.*, **23**, 676 (1983).
12. J. S. Chiou, J. W. Barlow, and D. R. Paul, *J. Appl. Polym. Sci.*, **30**, 1173 (1985).
13. W. E. Preston, J. W. Barlow, and D. R. Paul, *J. Appl. Polym. Sci.*, **29**, 845 (1984).
14. D. R. Paul, *J. Membr. Sci.*, **18**, 75 (1984).
15. W. R. Vieth, J. M. Howell, and J. H. Hsieh, *J. Membr. Sci.*, **1**, 177 (1976).
16. D. R. Paul, Ber. Bunsenges. *Phys. Chem.*, **83**, 294 (1979).
17. J. S. Chiou, J. W. Barlow, and D. R. Paul, *J. Appl. Polym. Sci.*, **30**, 2633 (1985).
18. J. S. Chiou, J. W. Barlow, and D. R. Paul, *J. Appl. Polym. Sci.*, **30**, 3911 (1985).
19. J. S. Chiou and D. R. Paul, *J. Appl. Polym. Sci.*, to appear.
20. D. R. Paul, *J. Polym. Sci., A-2*, **7**, 1811 (1969).
21. W. J. Koros, D. R. Paul, and A. A. Rocha, *J. Polym. Sci., Polym. Phys. Ed.*, **14**, 687 (1976).
22. W. J. Koros and D. R. Paul, *J. Polym. Sci., Polym. Phys. Ed.*, **14**, 1903 (1976).
23. A. G. Wonders and D. R. Paul, *J. Membr. Sci.*, **5**, 63 (1979).
24. D. R. Paul and J. O. Altamirano, *Adv. Chem. Ser.*, **142**, 371 (1975).
25. G. DiPaola-Baranji, S. J. Fletcher, and P. Degre, *Macromolecules*, **15**, 885 (1982).
26. B. Morra and R. S. Stein, *J. Polym. Sci., Polym. Phys. Ed.*, **20**, 2243 (1982).
27. J. Mijovic, H. L. Luo, and C. D. Han, *Polym. Eng. Sci.*, **22**, 234 (1982).
28. G. J. Welch and R. L. Miller, *J. Polym. Sci., Polym. Phys. Ed.*, **14**, 1683 (1976).
29. K. Nakagawa and Y. Ishida, *Kolloid Z.*, **251**, 103 (1973).
30. W. J. Koros, A. H. Chan, and D. R. Paul, *J. Membr. Sci.*, **2**, 165 (1977).
31. A. S. Michaels and R. B. Parker, Jr., *J. Polym. Sci.*, **41**, 53 (1959).
32. A. S. Michaels and H. J. Bixler, *J. Polym. Sci.*, **50**, 393 (1961).
33. D. R. Paul, J. W. Barlow, R. E. Bernstein, and D. C. Wahrmund, *Polym. Eng. Sci.*, **18**, 1225 (1978).
34. J. M. Prausnitz and F. H. Shair, *AIChE J*, **7**, 682 (1961).
35. W. J. Koros, D. R. Paul, M. Fujii, H. B. Hopfenberg, and V. T. Stannett, *J. Appl. Polym. Sci.*, **21**, 2899 (1977).
36. G. S. Huvard, V. T. Stannett, W. J. Koros, and H. B. Hopfenberg, *J. Membr. Sci.*, **6**, 185 (1980).
37. A. J. Erb and D. R. Paul, *J. Membr. Sci.*, **8**, 11 (1981).

38. J. H. Petropoulos, *J. Polym. Phys., A-2,* **8**, 1797 (1970).
39. W. J. Koros and D. R. Paul, *J. Polym. Sci., Polym. Phys. Ed.,* **14**, 675 (1976).
40. G. B. Okonishnikov and V. P. Shripov, *Vysokomol. Soedin., Ser. B,* **15**, 890 (1973).
41. J. S. Chiou, Ph.D. dissertation, University of Texas at Austin, 1985.
42. D. R. Kemp and D. R. Paul, *J. Polym. Sci.,* **41C**, 79 (1973).
43. A. S. Michaels and H. J. Bixler, *J. Polym. Sci.,* **50**, 413 (1961).
44. K. Toi, G. Morel, and D. R. Paul, *J. Appl. Polym. Sci.,* **27**, 2997 (1982).
45. M. J. El-Hibri and D. R. Paul, *J. Appl. Polym. Sci.*, **30**, 3649 (1985).
46. H. J. Bixler and O. J. Sweeting, in *The Science and Technology of Polymer Films*, O. J. Sweeting, Ed., Wiley-Interscience, New York, 1968, Vol. II, Chap. 1.
47. W. H. Burgess, H. B. Hopfenberg, and V. T. Stannett, *J. Macromol. Sci. Phys.,* **B5**, 23 (1971).
48. K. Toi, Y. Maeda, and T. Tokuda, *J. Membr. Sci.,* **13**, 15 (1983).
49. Y. Maeda, Ph.D. dissertation, University of Texas at Austin, 1985.
50. G. J. Van Amerongen, *J. Polym. Sci.,* **5**, 307 (1950).
51. R. B. Bird, W. E. Stewart, and E. N. Lightfoot, *Transport Phenomena*, Wiley, New York, 1966, p. 744.
52. M. J. El-Hibri, Ph.D. dissertation, University of Texas at Austin, 1985.
53. D. W. Breck, *Zeolite Molecular Seives*, Wiley, New York, 1974.

Received April 19, 1985
Accepted July 18, 1985